Engineering Analysis with Boundary Elements 76 (2017) 69–79

Contents lists available at ScienceDirect

Engineering Analysis with Boundary Elements

journal homepage: www.elsevier.com/locate/enganabound

Numerical simulation of three-dimensional double-diffusive natural convection in porous media by boundary element method

J. Kramer Stajnko*, J. Ravnik, R. Jecl

Faculty of Civil Engineering, Transportation Engineering and Architecture, Faculty of Mechanical Engineering, University of Maribor, Smetanova 17, SI-2000 Maribor, Slovenia

ARTICLE INFO

Keywords:
Double-diffusive natural convection
Porous media
Boundary element method
Brinkman-extended Darcy formulation

ABSTRACT

The paper presents numerical results for three-dimensional double-diffusive natural convection in a cubic enclosure fully filled with fluid saturated porous media. Two opposite vertical walls of the enclosure are subjected to different values of temperature and concentration, which causes buoyant and diffusive flow in the porous media domain. Mathematical model is based on the Brinkman-extended Darcy formulation as a governing momentum equation, which is coupled with the energy and species equations. The three-dimensional boundary element method based solver was used to solve the obtained set of partial differential equations. The existing numerical algorithm primarily derived for the pure fluid flow simulations was adopted to simulate transport phenomena in porous media. It is based on the combination of single and subdomain boundary element method, which solves the velocity-vorticity formulation of the governing equations. In the paper the influence of some governing parameters, specially the Rayleigh number, Darcy number and buoyancy coefficient are investigated in order to analyze the heat and mass transfer through porous enclosure. The numerical code is verified by comparison of the results with available previous numerical data found in the literature.

1. Introduction

Problems of double-diffusive natural convection in porous media occur in many natural and engineering applications and have been recently intensively investigated. Enhanced attention has been dedicated to several environmental problems, e.g. transport of contaminant through water saturated soil in field of protection of groundwater resources and nuclear waste disposals. In such problems complex flow patterns are a result of combined actions of temperature and concentration gradients and the presence of porous media. There are many published analytical, numerical as well as experimental studies considering simultaneous heat and solute transfer in several different configurations of porous media domains. First, most commonly studied situation is the horizontal porous layer subjected to vertical temperature and concentration gradients. The critical conditions for the onset of convective motion were usually obtained on the basis of linear stability analysis. Murray and Chen [1] published a study where double-diffusive natural convection in horizontal porous layer is investigated experimentally. They reported about dramatic behavior of flow patterns in case when performing the double-diffusive experiments, with occurrence of three-dimensional cells. Trevisan and Bejan [2] studied the critical conditions for the onset of convective motion in an infinite horizontal porous layer. Rosenberg and Spera [3] published a study with numerical results of convection in porous medium heated from below with two opposing sources of buoyancy. They studied in detail the effect of Rayleigh number, Lewis number and buoyancy coefficient on the overall heat and mass transfer. Amahmid et al. [4] studied double-diffusive parallel flow analytically and numerically, where the analytical solution is based on the parallel flow approximation. The critical Rayleigh number for the onset of parallel flow is determined analytically as a function of Lewis number, buoyancy coefficient and Darcy number. Mahidjiba et al. [5] published numerical study of double-diffusive natural convection in a horizontal porous cavity using the linear stability analysis.

The second common configuration is the vertical cavity fully filled with saturated porous media where the vertical walls are maintained at horizontal temperature and concentration gradients. Two different types of phenomena which were studied can be found, namely the resulting thermal and solutal buoyancy forces can have aiding or opposing influence on each other. Trevisan and Bejan [6,7,2] published comprehensive analytical and numerical studies considering double-diffusive natural convection in a porous enclosure where the vertical walls are maintained at different temperature and concentration values or uniform heat and mass fluxes. The developed analytical solutions are

* Corresponding author.
E-mail addresses: janja.kramer@um.si (J.K. Stajnko), jure.ravnik@um.si (J. Ravnik), renata.jecl@um.si (R. Jecl).

http://dx.doi.org/10.1016/j.enganabound.2016.12.007
Received 9 November 2015; Received in revised form 16 December 2016; Accepted 20 December 2016

Nomenclature

α	effective thermal diffusivity of porous medium, $\alpha_e = \lambda_e/c_f$
β_C	volumetric expansion coefficient due to chemical species
β_T	volumetric thermal expansion coefficient
Γ	boundary of the computational domain
Λ	viscosity ratio, $\Lambda = \mu_{eff}/\mu$
λ_e	effective thermal conductivity of fluid saturated porous medium, $\lambda_e = \phi\lambda_f + (1-\phi)\lambda_s$
λ_f	thermal conductivity of fluid
λ_s	thermal conductivity of solid phase
μ	fluid dynamic viscosity
μ_{eff}	effective viscosity
ν	kinematic viscosity of the fluid
Ω	computational domain
ϕ	porosity
ρ	density
σ	heat capacity ratio
Θ	inner angle
$u^\star$	fundamental solution of the Laplace equation
$\vec{\omega}$	vorticity vector
$\vec{\xi}$	source or collocation point
$\vec{g}$	acceleration due to gravity
$\vec{n}$	unit normal vector
$\vec{r}$	position vector
$\vec{v}$	velocity vector
C	concentration
$c(\vec{\xi})$	geometric coefficient
c_f	heat capacity for fluid phase, $c_f = (\rho c_p)_f$
c_p	specific heat at constant pressure
c_s	heat capacity for solid phase, $c_s = (\rho c_p)_s$
D	mass diffusivity
Da	Darcy number
Eu	Euler number
K	permeability
L	characteristic length
Le	Lewis number
N	buoyancy coefficient
Nu	Nusselt number
p	pressure
Pr	Prandtl number
Ra_p	porous thermal Rayleigh number, $Ra_p = Ra_T \cdot Da$
Ra_S	solutal Rayleigh number
Ra_T	thermal Rayleigh number
Re_p	pore Reynolds number
Sh	Sherwood number
T	temperature
t	time
v_0	characteristic velocity

validated with several numerical simulations for various governing parameters. Alavyoon [8] published a study where the unsteady and steady convection in a vertical enclosure with applied constant fluxes of heat and mass on the vertical walls is considered. Several comparisons between the fully numerical and analytical solutions for different range of governing parameters are reported. Similar study, where the results of steady state calculations in porous media subjected to uniform fluxes of heat and mass, was published by Mamou et al. [9]. Authors investigated the influence of Rayleigh number, Lewis number and buoyancy coefficient on overall heat and mass transfer in porous enclosure. A comprehensive numerical study was published by Goyeau et al. [10] focusing on the situations with cooperating thermal and solutal buoyancy forces. Nithiarasu et al. [11] studied double-diffusive natural convective flow within a rectangular enclosure with prescribed values of temperature and concentration on the vertical walls, using the generalized porous medium approach. Karimi-Fard et al. [12] investigated the influence of different flow models for porous media on an example of double-diffusive natural convection in a square porous cavity. Bennacer et al. [13] studied the same configuration filled with anisotropic porous media. Recently, Kramer et al. [14] published a numerical study with several results of double-diffusive convective flow in porous cavity obtained with the boundary element method. However, the boundary element method has already been used for the simulations of steady state natural convection problem in porous media, with dual reciprocity transformation of the domain integrals, namely for the Darcy model in Šarler et al. [15] and furthermore, for the Darcy-Brinkman model in Šarler et al. [16].

All of the above mentioned studies are confined on the examples of two-dimensional problems. The studies considering three-dimensional analysis of convective flow due to combined action of thermal and solutal buoyancy forces in different porous media configurations are limited. Sezai and Mohamad [17] published a study, where a three-dimensional geometry of porous media domain is considered, focusing on the case with the opposing effects of buoyancy forces. The results show three-dimensional behavior of the flow for certain parameter ranges with secondary flow formations which can not be captured with two-dimensional models. Similar study presenting some results of the opposed action of thermal and solutal buoyancy forces was published recently by Kramer et al. [18]. Furthermore, the effects of lateral aspect ratio on three-dimensional geometries were studied by Mohamad et al. [19].

The present paper considers a problem of double-diffusive natural convection in a three-dimensional porous media domain using the boundary element method solver. The mathematical model is given at the beginning which is based on the Navier-Stokes equations suitable modified for the simulations of porous media flow, where the Brinkman-extended Darcy formulation is used as a momentum equation. In addition, the boundary element method is briefly outlined. Since all of the above mentioned existing studies are limited in a manner that they are presenting the results of the classical Darcy model and are focused on the effects of opposing gradients of temperature and concentration, in this paper the numerical results of three-dimensional model, revealing the influence of different values of Darcy number and buoyancy coefficient (for the cases of opposing as well as cooperating temperature and concentration gradients) at fixed values of thermal Rayleigh number and Lewis number on the convective motion regime, are studied. The influence of the parameters on the occurrence of three-dimensional flow patterns is investigated.

2. Mathematical model

The problem under consideration is double-diffusive natural convection in a three-dimensional cavity, filled with porous medium which is fully saturated with binary fluid (e.g. aqueous solutions). Two opposite vertical walls are maintained at different temperatures (T_1 and T_2) and concentrations (C_1 and C_2), while the rest of the walls are adiabatic and impermeable.

The mathematical description of the problem is based on the conservation laws for mass, momentum, energy and species concentration, primarily written at the microscopic level, describing the pure fluid flow. In general, that kind of model is not appropriate to describe the fluid flow within the porous media domain, since the geometry is irregular and complex. With an averaging procedure over the representative elementary volume (REV) all flow quantities can be written as volume-averaged values, which enables amenable theoretical treatment. Every macroscopic variable is defined as an appropriate mean

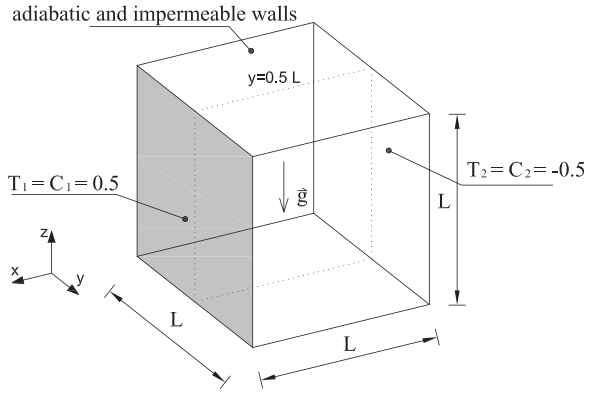

Fig. 1. Geometry of the problem.

over the REV, which in general, has to be much larger than the pore scale and considerably smaller than the length scale of the macroscopic flow domain. All details about the averaging procedure are given in [20] and are omitted in this paper.

To simplify the mathematical description, following assumptions are adopted: the flow is laminar and steady, the binary fluid is Newtonian and incompressible, where the fluid density depends only on the temperature and concentration variations which can be described with the Oberbeck Boussinesq approximation as:

$$\rho = \rho_0(1 - \beta_T(T - T_0) - \beta_C(C - C_0)), \tag{1}$$

where subcscript 0 refers to a reference state.

Volumetric thermal expansion coefficient, β_T and volumetric expansion coefficient due to chemical species, β_C are given with expressions:

$$\beta_T = -\frac{1}{\rho}\left[\frac{\partial\rho}{\partial T}\right]_C, \quad \beta_C = -\frac{1}{\rho}\left[\frac{\partial\rho}{\partial C}\right]_T. \tag{2}$$

The solid phase of the porous media domain is assumed to be isotropic, homogeneous and in thermodynamic equilibrium with the fluid phase. Furthermore, the Soret and Dufour effects are assumed to be negligible.

The macroscopic conservation equations describing transport phenomena in porous media domain are given in non-dimensional form using following dimensionless variables for velocity $\vec{v}$, position vector $\vec{r}$, time t, gravitational acceleration $\vec{g}$, pressure p, temperature T, and concentration C:

$$\vec{v} \to \frac{\vec{v}}{v_0}, \quad \vec{r} \to \frac{\vec{r}}{L}, \quad t \to \frac{v_0 t}{L}, \quad \vec{g} \to \frac{\vec{g}}{g_0}, \quad p \to \frac{p}{p_0},$$
$$T \to \frac{(T - T_0)}{\Delta T}, \; C \to \frac{(C - C_0)}{\Delta C}. \tag{3}$$

The term v_0 is characteristic velocity given with an expression common for buoyant flow simulations as $v_0 = \lambda_f/(\rho c_p)_f L$, where λ_f is fluid thermal conductivity, $(\rho c_p)_f$ is heat capacity for fluid phase and L is characteristic length (e.g. length of one side of cubic cavity). Furthermore, T_0 and C_0 are characteristic temperature and concentration ($T_0 = (T_2 - T_1)/2$, $C_0 = (C_2 - C_1)/2$), ΔT and ΔC are characteristic temperature and concentration differences ($\Delta T = T_2 - T_1$, $\Delta C = C_2 - C_1$), p_0 is characteristic pressure $p_0 = 1bar$, while gravitational acceleration is $g_0 = 9.81\ m/s^2$.

According to the above dimensionless parameters, the macroscopic governing conservation equations for mass, momentum, energy and species, can be written as:

$$\vec{\nabla}\cdot\vec{v} = 0, \tag{4}$$

$$\frac{1}{\phi}\frac{\partial\vec{v}}{\partial t} + \frac{1}{\phi^2}(\vec{v}\cdot\vec{\nabla})\vec{v} = -Ra_T\ Pr\,(T + N\ C)\vec{g} - \frac{1}{Eu}\vec{\nabla}p + \frac{1}{\phi}Pr\nabla^2\vec{v} - \frac{Pr}{Da}\vec{v}, \tag{5}$$

$$\sigma\frac{\partial T}{\partial t} + (\vec{v}\cdot\vec{\nabla})T = \frac{\lambda_e}{\lambda_f}\nabla^2 T, \tag{6}$$

$$\phi\frac{\partial C}{\partial t} + (\vec{v}\cdot\vec{\nabla})C = \frac{1}{Le}\nabla^2 C, \tag{7}$$

where:

- Ra_T is thermal fluid Rayleigh number, $Ra_T = g\beta_T\Delta TL^3/\nu\alpha$,
- Pr is Prandtl number, $Pr = \nu/\alpha$,
- N is buoyancy coefficient, $N = Ra_S/Ra_T$, where $Ra_S = g\beta_C\Delta CL^3/\nu\alpha$ is solutal Rayleigh number,
- Eu is Euler number, $Eu = \rho v^2/p$,
- Da is Darcy number, $Da = K/L^2$,
- Le is Lewis number, $Le = \alpha/D$.

Additionally the porous Rayleigh number (Ra_P) is defined, which links the thermal Rayleigh and Darcy numbers:

- $Ra_p = Ra_T{\cdot}Da$.

The parameter α in the above expressions represents the effective thermal diffusivity of porous medium $\alpha = \lambda_e/c_f$, while D is the mass diffusivity.

The momentum Eq. (5) represents the Brinkman-extended Darcy model where the Forchheimer inertia term has been neglected. This model is valid only for the case of low velocity, where the inertial effects are negligible. In that case the pore Reynolds number is given as $Re_p{=}\rho vK^{0.5}\mu$ (where the characteristic length is represented as the square root of the permeability) and its value is less than unity [21].

The Brinkman viscous term (third on the r.h.s. of Eq. (5)) is analogous to the Laplacian term in the classical Navier-Stokes equations for the case of pure fluid flow and is originally given with the coefficient $\Lambda = \mu_{eff}/\mu$, which represents the ratio of the effective viscosity to fluid viscosity. In this study the viscosity ratio is adopted to be $\Lambda = 1/\phi$ as suggested in [22].

In the energy Eq. (6), σ is specific heat ratio, defined as $\sigma = (\phi c_f + (1 - \phi)c_s)/c_f$, where $c_f = (\rho c_p)_f$ and $c_s = (\rho c_p)_s$ are heat capacities for fluid and solid phase respectively.

2.1. Velocity-vorticity formulation

The governing set of equations is transformed by introduction of the velocity-vorticity formulation which separates the computational scheme into the kinematic and kinetic computational parts. The vorticity vector is introduced as the curl of the velocity, $\vec{\omega} = \vec{\nabla}\times\vec{v}$, where both, velocity and vorticity fields are solenoidal by the definition, $\vec{\nabla}\cdot\vec{v} = 0$, $\vec{\nabla}\cdot\vec{\omega} = 0$. The kinematics equation is a vector elliptic partial differential equation of Poisson type and is obtained from the mass conservation law (4) as:

$$\nabla^2\vec{v} + \vec{\nabla}\times\vec{\omega} = 0, \tag{8}$$

By applying the curl operator to the momentum Eq. (5), the vorticity transport equation can be derived:

$$\phi\frac{\partial\vec{\omega}}{\partial t} + (\vec{v}\cdot\vec{\nabla})\vec{\omega} = (\vec{\omega}\cdot\vec{\nabla})\vec{v} - PrRa_T\phi^2\vec{\nabla}\times(T + N\ C)\vec{g} + Pr\phi\nabla^2\vec{\omega} - \frac{Pr}{Da}\phi^2\vec{\omega}, \tag{9}$$

which is representing the kinetic computational part together with the energy and species transport equations.

The pressure appears in the general momentum Eq. (5) in the gradient form and as such it can cause numerical instabilities. In the velocity-vorticity formulation the pressure term is eliminated from the momentum equation as a primary variable, as a consequence of applying the curl operator.

Table 1
Variations of Nusselt number with different grid sizes and various Darcy number values.

	Mesh	Number of nodes	Ra_P=100, Le=0, N=0				
		Da	10^{-1}	10^{-2}	10^{-3}	10^{-4}	10^{-5}
2D	20 ×20	1681	1.0639	1.6329	2.3697	2.8756	3.1656
	30×30	3721	1.0638	1.6331	2.3680	2.8537	3.1503
3D	12 × 12 × 12	15625	1.0423	1.5428	2.3432	2.9784	3.3008
	20 × 8 × 20	28577	1.0394	1.5329	2.3313	2.9575	3.2950
	22 × 10 × 22	42525	1.0393	1.5327	2.3307	2.9552	3.2945
	30 × 10 × 30	78141	1.0393	1.5325	2.3303	2.9541	3.2934

Table 2
Nusselt number values for the 3D natural convection in a cubic enclosure for Ra_P=1000, ϕ = 0.8 and different values of Darcy number. The results are compared to study [31].

Ra_P=1000; Le=0; N=0					
Da	10^{-2}	10^{-3}	10^{-4}	10^{-5}	10^{-6}
Present	**3.770**	**6.922**	**10.558**	**13.242**	**14.568**
Sharma and Sharma[31]	3.99	6.95	10.14	12.78	13.72

Table 3
Nusselt and Sherwood number values for 3D natural convection in a cubic enclosure for Ra_P=10, $Da = 10^{-6}$, $N = -0.5$ and different values of Lewis number. The reference results are from the study [19].

Ra_P=10; $Da = 10^{-5}$; $N = -0.5$				
		Le=1	Le=10	Le=100
Nu	Present	**1.019**	**1.039**	**1.048**
	[19]	1.0198	1.0404	1.0424
Sh	Present	**1.019**	**2.450**	**4.743**
	[19]	1.0198	2.4467	4.7511

Table 4
Nusselt and Sherwood number values for 3D natural convection in a cubic enclosure for Ra_P=1, $Da = 10^{-6}$, Le=50 and different values of buoyancy coefficient. The reference results are from the study of Mohamad et al. [19].

Ra_P=1; $Da = 10^{-6}$; Le=50			
		$N = -0.2$	$N = -0.5$
Nu	Present	**1.0005**	**1.0002**
	[19]	1.0006	1.0003
Sh	Present	**1.9627**	**1.5524**
	[19]	1.9517	1.5495

Table 6
Nusselt and Sherwood number values for 3D natural convection in a cubic enclosure for Le=10 and N=1 and different values of Da, Ra_p and Ra_T.

Le=10, N=1				
Ra_T	Ra_p	Da	Nu	Sh
10^5	10	10^{-4}	1.025	2.937
	100	10^{-3}	2.755	9.744
	1000	10^{-2}	3.226	18.696
10^6	10	10^{-5}	1.051	3.103
	100	10^{-4}	3.563	13.527
	1000	10^{-3}	6.148	25.557
10^7	10	10^{-6}	1.082	3.852
	100	10^{-5}	4.101	16.897
	1000	10^{-4}	10.447	30.186

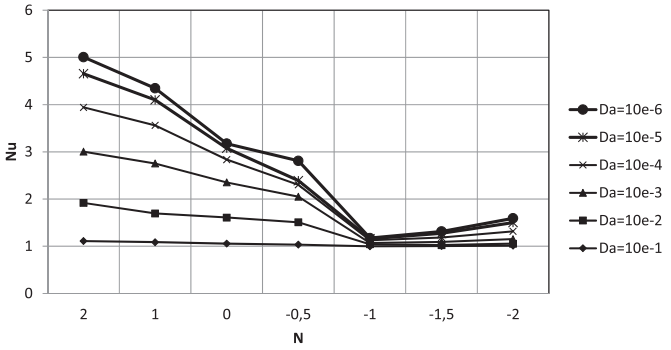

Fig. 2. Nusselt number values depending on buoyancy coefficient for Ra_p = 100, Le = 10 and various Da.

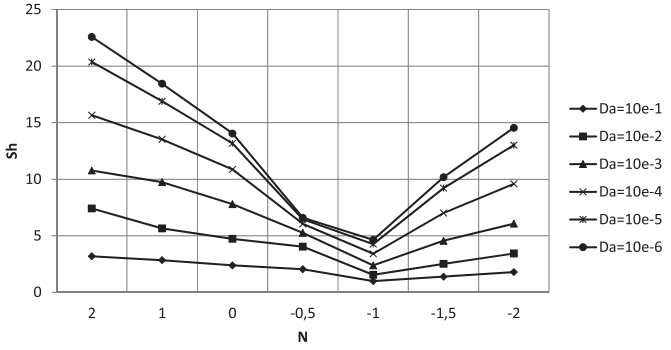

Fig. 3. Sherwood number values depending on buoyancy coefficient for Ra_p = 100 , Le = 10 and various Da.

The obtained set of partial differential Eqs. (8), (9), (6) and (7) forms a nonlinear system of equations for the unknown velocity, vorticity, temperature and concentration fields. The problem of heat

Table 5
Nusselt and Sherwood number values for 3D natural convection in a cubic enclosure for $Da = 10^{-6}$, Le=10, $N = -0.5$ and different values of Ra_p. The reference results are from the study of Sezai and Mohamad [17].

$Da = 10^{-6}$; Le=10; $N = -0.5$									
	Ra_p	1	5	10	50	100	200	500	1000
Nu	Present	**1.000**	**1.021**	**1.039**	**1.566**	**2.391**	**3.568**	**6.397**	**10.984**
	[17]	1.0	1.0	1.0	1.6	2.4	3.4	6.4	–
Sh	Present	**1.019**	**1.392**	**2.450**	**4.873**	**6.473**	**8.157**	**12.105**	**25.550**
	[17]	1.0	1.5	2.4	4.9	6.2	8.2	11.9	–

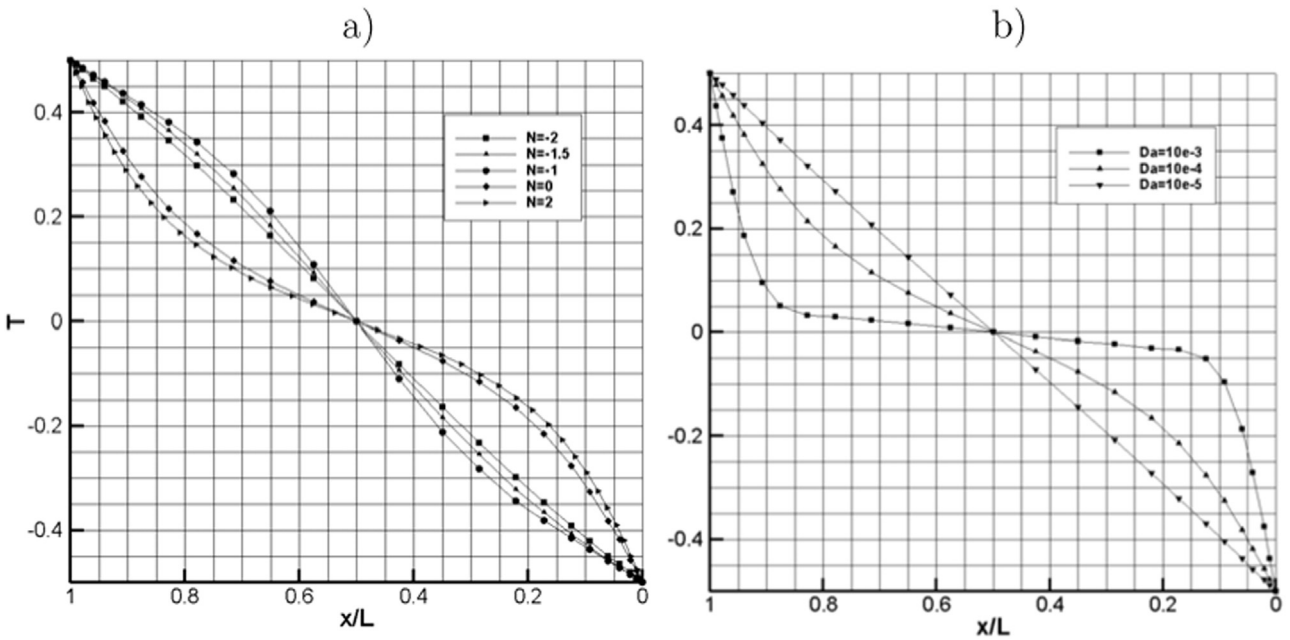

Fig. 4. Temperature profiles at $y = 0.5$ and $z = 0.5$; (a) $Ra_T = 10^6$, $Da = 10^{-4}$, $Le = 10$ and various N; (b) $Ra_T = 10^6$, $N = 0$, $Le = 10$ and various Da.

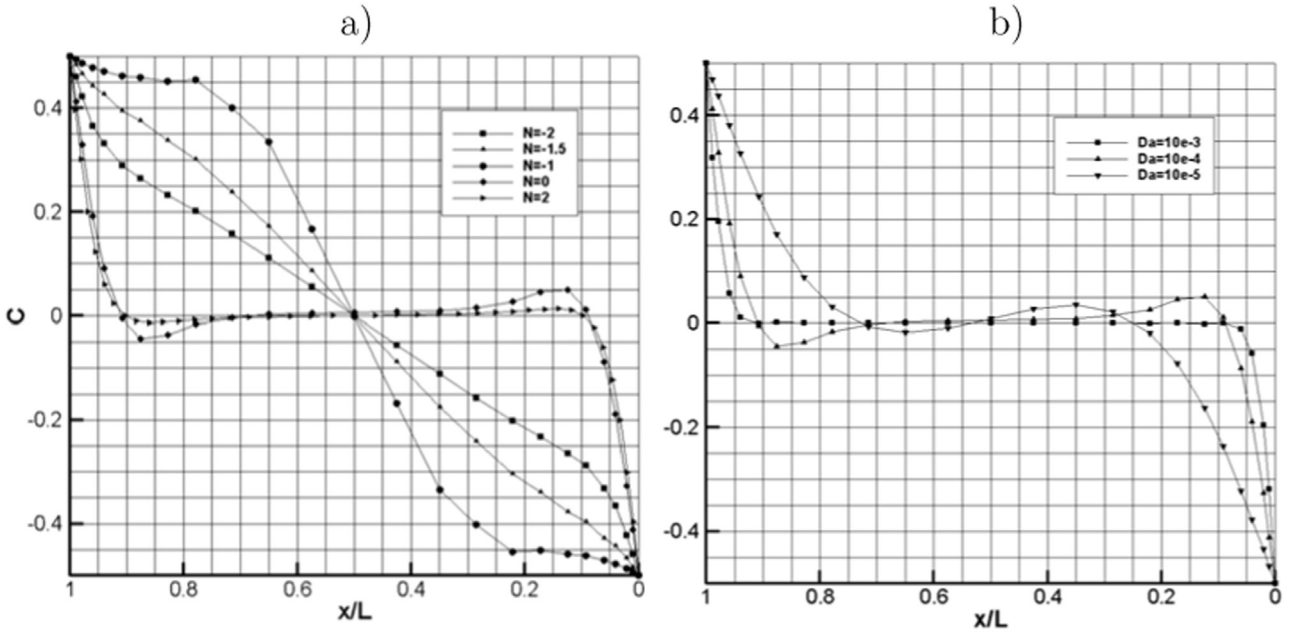

Fig. 5. Concentration profiles at $y = 0.5$ and $z = 0.5$; (a) $Ra_T = 10^6$, $Da = 10^{-4}$, $Le = 10$ and various N; (b)$Ra_T = 10^6$, $N = 0$, $Le = 10$ and various Da.

and mass transfer in porous media domain is uniquely defined by specifying the buoyancy coefficient, fluid Rayleigh, Prandtl, Lewis and Darcy numbers together with the appropriate initial and boundary conditions.

3. Numerical method

The numerical method used to perform simulations in this paper is based on the solution of velocity-vorticity formulation of Navier-Stokes equations, using a combination of a single domain BEM and sub-domain BEM. Sub-domain BEM is used to solve the vorticity, energy and species transport equations. Because it is based on domain decomposition, the matrices arising in discretization are sparse and the efficiency of the solution is comparable to FVM or FEM [23]. The kinematics equation, which is used to determine the vorticity boundary conditions, is due to the restrictions of the Biot-Savart law, solved by single domain BEM, which results in a full system of equations. This limits the maximum grid size due to memory constraints. This drawback can be mitigated by the use of fast BEM, where sparse approximation of full matrices are used [24]. The main advantage of using single domain BEM to obtain boundary vorticity values is that the algorithm conserves mass in complex geometries, which is not the case when using velocity derivatives to calculate boundary vorticity values.

The numerical algorithm is devised as follows. The boundary conditions of Dirichlet or/and Neumann type for velocity, temperature and concentration are known at the beginning and are used to solve the kinematics Eq. (8) for domain velocity values, energy Eq. (6) for domain temperature values and species Eq. (7) for domain concentration values. The boundary conditions for vorticity values are unknown at the beginning and are calculated as a part of the algorithm by single

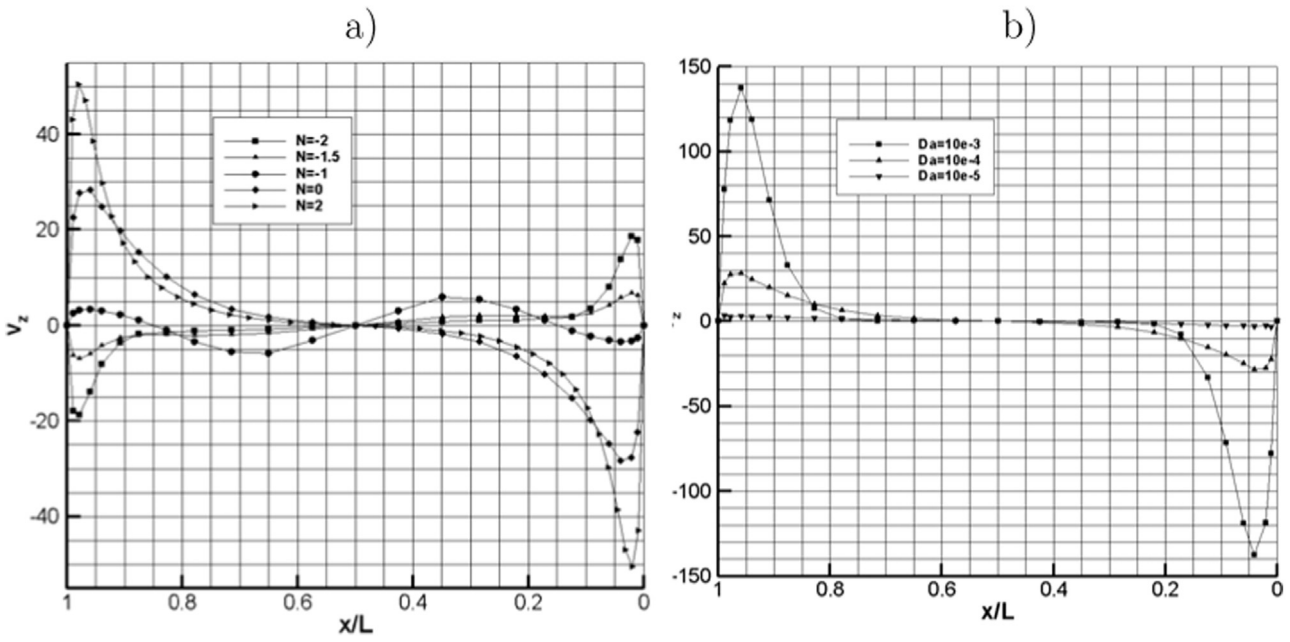

Fig. 6. Velocity profiles $v_z(x, 0.5L, 0.5L)$; (a) $Ra_T = 10^6$, $Da = 10^{-4}$, $Le = 10$ and various N; (b) for $Ra_T = 10^6$, $N = 0$, $Le = 10$ and various Da.

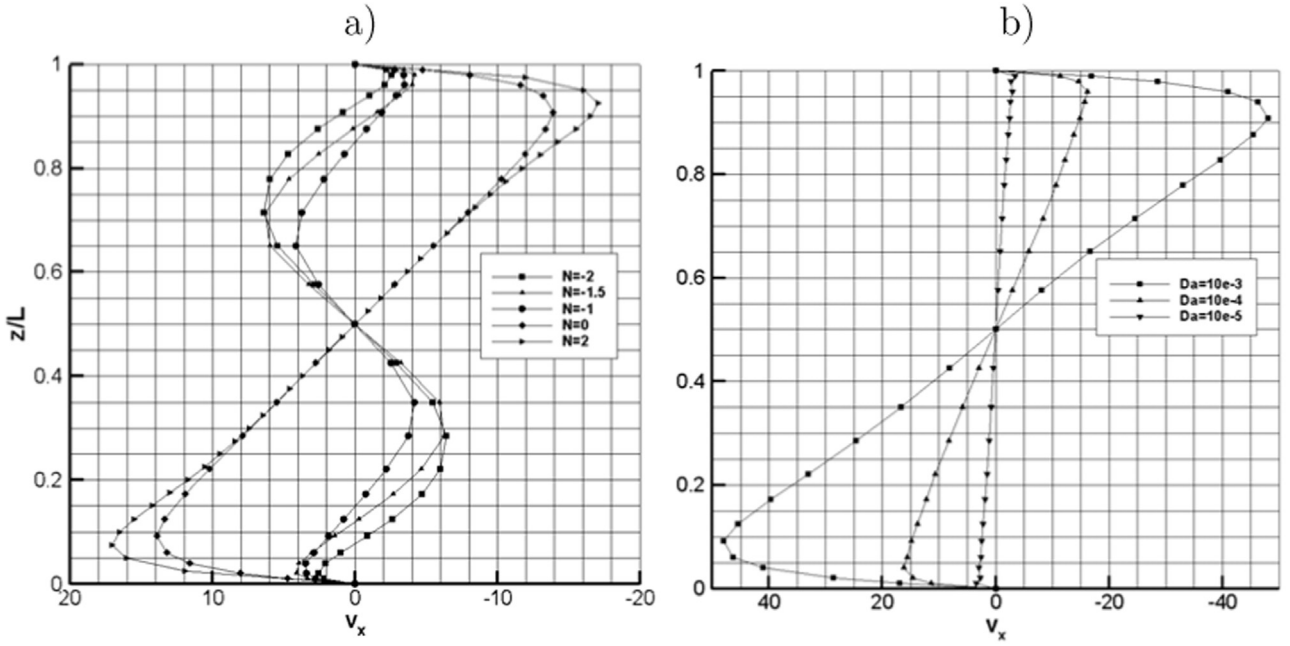

Fig. 7. Velocity profiles $v_x(0.5L, 0.5L, z)$; (a) $Ra_T = 10^6$, $Da = 10^{-4}$, $Le = 10$ and various N; (b) $Ra_T = 10^6$, $N = 0$, $Le = 10$ and various Da.

domain BEM out of the kinematics Eq. (8) [25]. The outline of the numerical algorithm is as follows:

1. Fluid and porous media properties are determined.
2. Vorticity values on the boundary are calculated by single domain BEM from the kinematics Eq. (8).
3. Velocity values within the domain are calculated by subdomain BEM from the kinematics Eq. (8).
4. Temperature values within the domain are calculated by subdomain BEM from the energy Eq. (6).
5. Concentration values within the domain are calculated by subdomain BEM from the concentration Eq. (7).
6. Vorticity values within the domain are calculated by subdomain BEM from the vorticity Eq. (9).
7. Check convergence. All steps from 2. until 6. are repeated until all flow fields achieve the required accuracy.

3.1. Integral form of governing equations

To solve the governing set of equations by BEM based algorithm the integral form of Eqs. (8), (9), (6) and (7) has to be obtained. Considering a domain Ω with a boundary Γ, the integral form of governing equations can be derived by using the Green's second identity for the unknown field function and for fundamental solution $u^\star$ of the Laplace equation: $u^\star = 1/4\pi|\vec{\xi} - \vec{r}|$, where $\vec{\xi}$ is source or collocation point on the boundary Γ and $\vec{r}$ a position vector in the domain Ω.

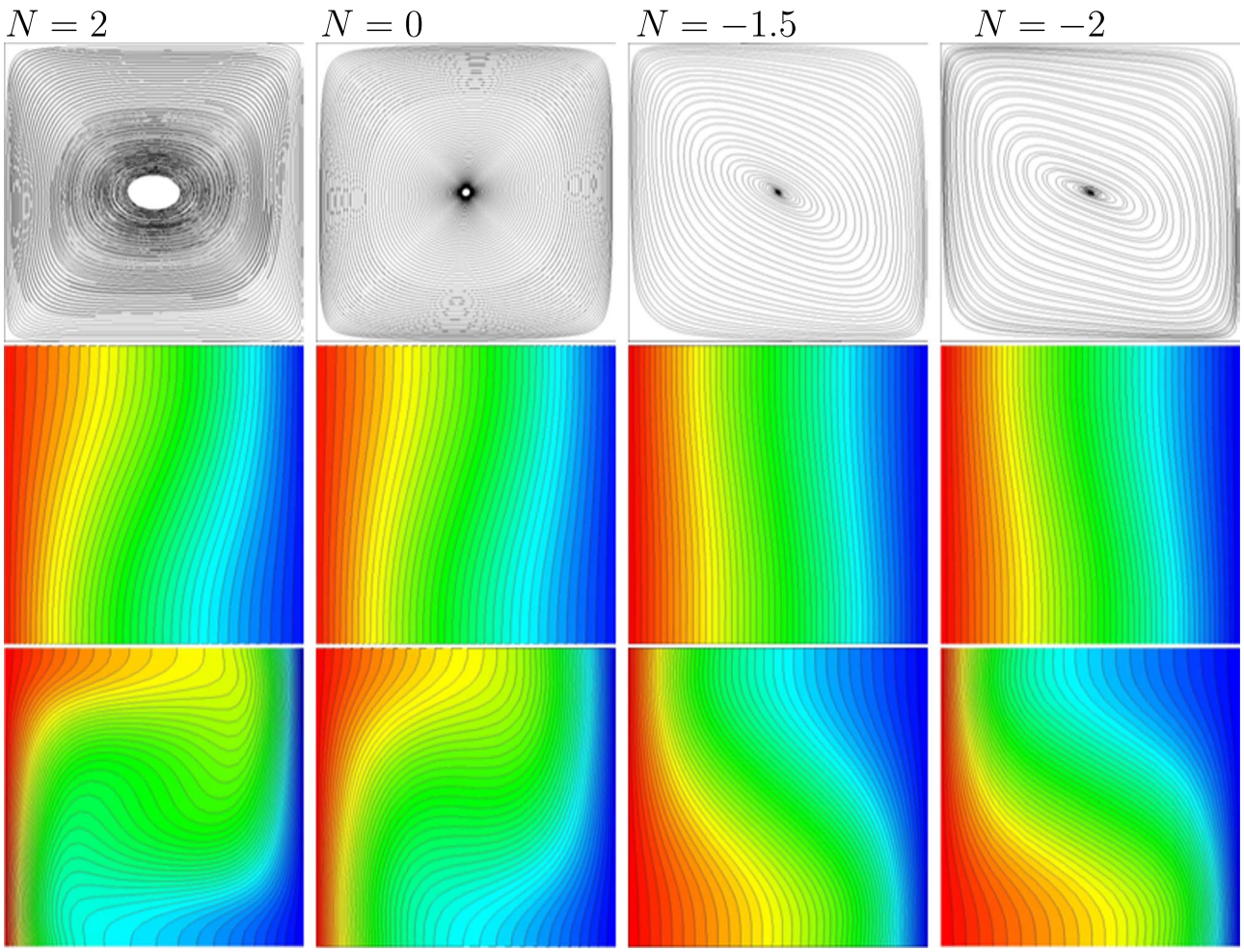

Fig. 8. Streamlines, temperature and concentration contour plots on the $y = 0.5L$ plane for $Ra_T = 10^3$, $Da = 10^{-1}$, $Le = 10$ and different values of N.

3.2. Integral representation of kinematics

The single domain BEM is first used to solve the kinematics Eq. (8) for the unknown boundary vorticity values. The integral form of the kinematics equation in tangential form is:

$$c(\vec{\xi})\vec{n}(\vec{\xi}) \times \vec{v}(\vec{\xi}) + \vec{n}(\vec{\xi}) \times \int_\Gamma \vec{v}\,\vec{\nabla}u^\star \cdot \vec{n}\, d\Gamma = \vec{n}(\vec{\xi}) \times \int_\Gamma \vec{v} \times (\vec{n} \times \vec{\nabla})u^\star d\Gamma + \vec{n}(\vec{\xi}) \times \int_\Omega (\vec{\omega} \times \vec{\nabla}u^\star) d\Omega, \tag{10}$$

where $c(\vec{\xi})$ is geometric factor defined as $c(\vec{\xi}) = \Theta/4\pi$, where Θ is the inner angle with origin in $\vec{\xi}$. Furthermore, $\vec{n}$ is a vector normal to the boundary, pointing out of the domain. After discretization the system matrix is formed in such way, that boundary values of vorticity are unknown, while domain vorticity and velocity values are taken from previous nonlinear iteration. The system is solved using a LU decomposition method. This approach has been proposed and used by Škerget [26–28].

To obtain the domain velocity values, the subdomain BEM has been used to solve the kinematics Eq. (8). The rewritten integral form is used as:

$$c(\vec{\xi})\vec{v}(\vec{\xi}) + \int_\Gamma \vec{v}(\vec{n}\cdot\vec{\nabla})u^\star d\Gamma = \int_\Gamma \vec{v} \times (\vec{n} \times \vec{\nabla})u^\star d\Gamma + \int_\Omega (\vec{\omega} \times \vec{\nabla}u^\star) d\Omega, \tag{11}$$

where the boundary values of velocity are known boundary conditions while the domain and boundary values of vorticity are known from the previous iteration.

3.3. Integral representation of kinetics

The same fundamental solution of the Laplace equation and a standard BEM derivation as in [29] are used to derive integral forms of the vorticity transport Eq. (9), energy transport Eq. (6) and species transport Eq. (7). In this work a natural convection phenomena is simulated for the cases of steady flow field, thus the time derivative terms in all equations $\partial\vec{\omega}/\partial t$, $\partial T/\partial t$ and $\partial C/\partial t$ are omitted. The final form of vorticity, energy and species transport equations are:

$$\begin{aligned} c(\vec{\xi})\omega_j(\vec{\xi}) + \int_\Gamma \omega_j \vec{\nabla}u^\star \cdot \vec{n}\, d\Gamma = {} & \int_\Gamma u^\star q_j d\Gamma \\ & + \frac{1}{Pr}\frac{1}{\phi}\int_\Gamma \vec{n}\cdot\{u^\star(\vec{v}\omega_j - \vec{\omega}v_j)\}\, d\Gamma \\ & - \frac{1}{Pr}\frac{1}{\phi}\int_\Omega (\vec{v}\omega_j - \vec{\omega}v_j)\cdot\vec{\nabla}u^\star d\Omega \\ & - Ra_T\phi\int_\Gamma (u^\star(T + N\ C)\vec{g} \times \vec{n})_j d\Gamma \\ & - Ra_T\phi\int_\Omega ((T + N\ C)\vec{\nabla} \times u^\star\vec{g})_j d\Omega \\ & + \frac{\phi}{Da}\int_\Omega \omega_j u^\star d\Omega, \end{aligned} \tag{12}$$

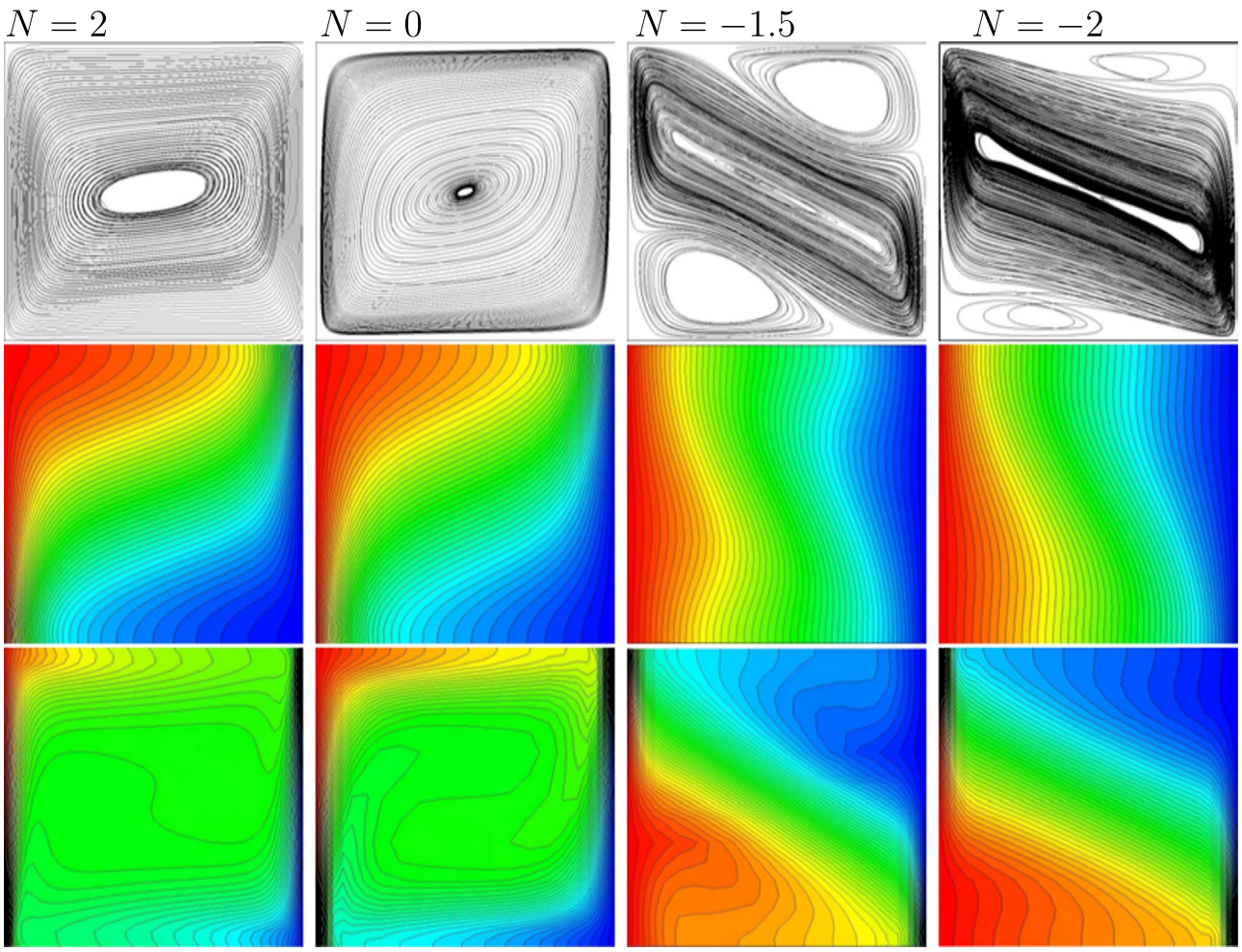

Fig. 9. Streamlines, temperature and concentration contour plots on the $y = 0.5L$ plane for $Ra_T = 10^5$, $Da = 10^{-3}$, $Le = 10$ and different values of N.

$$c(\vec{\xi})T(\vec{\xi}) + \int_\Gamma T\vec{\nabla}u^\star\cdot\vec{n}\,d\Gamma = \int_\Gamma u^\star q_T\,d\Gamma + \frac{\lambda_f}{\lambda_e}\left(\int_\Gamma \vec{n}\cdot\{u^\star(\vec{v}T)\}\,d\Gamma - \int_\Omega (\vec{v}T)\cdot\vec{\nabla}u^\star\,d\Omega\right), \tag{13}$$

$$c(\vec{\xi})C(\vec{\xi}) + \int_\Gamma C\vec{\nabla}u^\star\cdot\vec{n}\,d\Gamma = \int_\Gamma u^\star q_C\,d\Gamma + \frac{1}{Le}\left(\int_\Gamma \vec{n}\cdot\{u^\star(\vec{v}C)\}\,d\Gamma - \int_\Omega (\vec{v}C)\cdot\vec{\nabla}u^\star\,d\Omega\right). \tag{14}$$

In above equations, ω_j is a vorticity component, q_j is a component of vorticity flux, q_T and q_C are the heat and species fluxes, respectively.

In the subdomain BEM method a mesh of the entire domain Ω has to be made, where each mesh element is named a subdomain. All equations are written for each of the subdomains. The field functions and flux across the boundary and within the domain are interpolated using shape functions. In this work a hexahedral mesh elements with a standard shape functions for a 27 node Lagrangian domain are used. The field functions on each element are interpolated using continuous quadratic interpolation, while the fluxes are interpolated using the discontinuous linear interpolation.

The presented algorithm has been proposed for the case of 3D fluid flow by Ravnik et. al [25,27] and later adopted for the simulation of 3D nanofluid flow [28] and 3D porous media flow [30]. In the present work the algorithm is expanded for the case of double-diffusive natural convection with additional species equation, furthermore, porous media parameters were introduced in all equations.

4. Test case

The numerical simulations of double-diffusive natural convection were performed on the example of cubic cavity, filled with fluid saturated porous media and subjected to a temperature and concentration differences on two opposite vertical walls, while the rest of the walls were adiabatic and impermeable. The geometry with boundary conditions are shown in Fig. 1. Due to applied temperature and concentration gradients, density differences are induced which results in appearance of thermal and solutal buoyancy forces. The flow regime in the cavity is strongly dependant on the interaction between the thermal and solutal buoyancy forces, which can be either cooperating or opposing.

The heat and mass transfer through porous media is expected to depend on several fluid and porous media properties, such as porosity, permeability, thermal conductivity, species diffusivity, heat and solute capacitance, etc. In order to compare different conditions on overall heat and mass transfer through porous media domain, wall heat flux and wall species flux are calculated, which are expressed in terms of dimensionless Nusselt and Sherwood numbers as:

$$Nu = \int_\Gamma \vec{\nabla}T\cdot\vec{n}\,d\Gamma\ , \quad Sh = \int_\Gamma \vec{\nabla}C\cdot\vec{n}\,d\Gamma, \tag{15}$$

where Γ is the surface through which the heat flux and species flux are

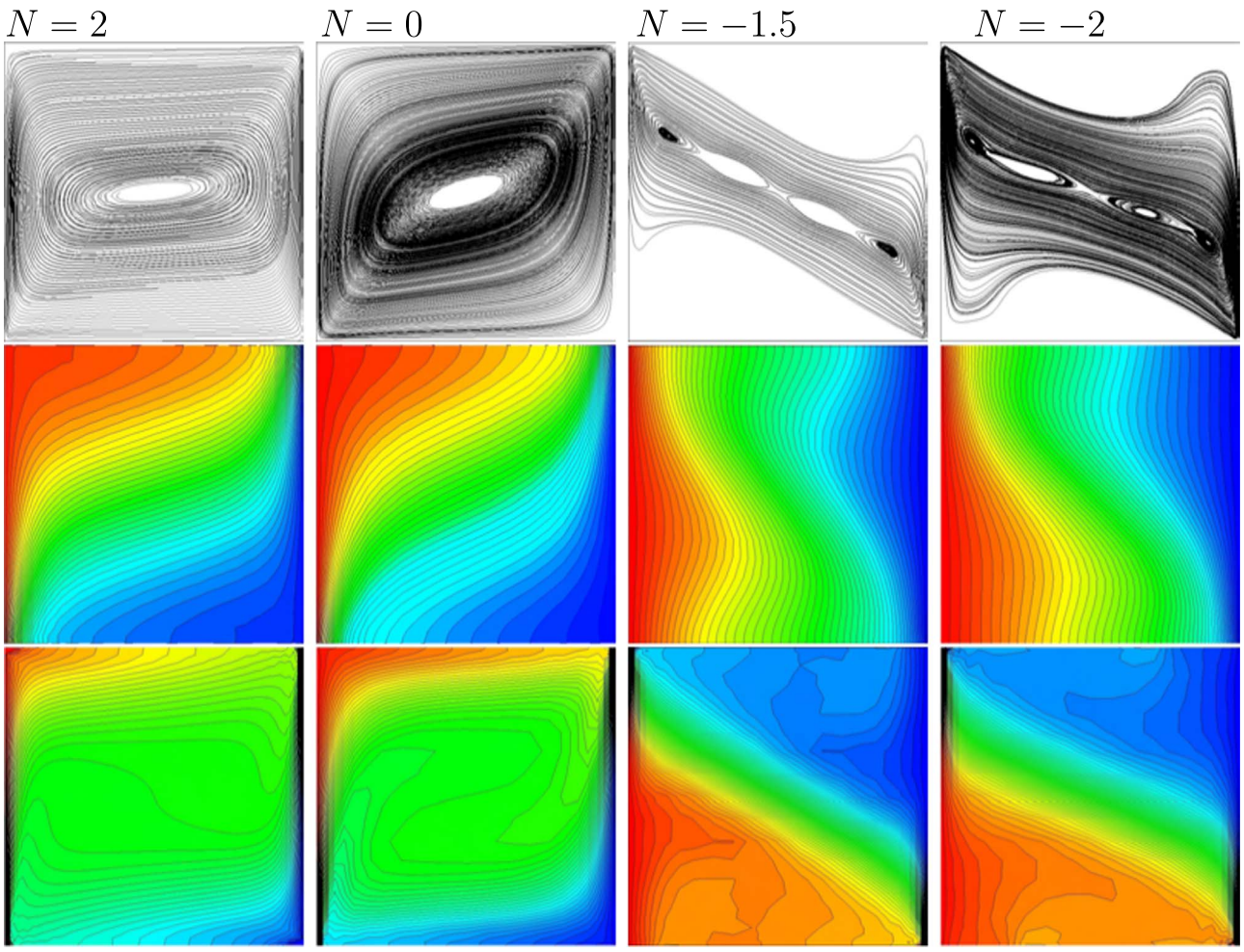

Fig. 10. Streamlines, temperature and concentration contour plots on the $y = 0.5L$ plane for $Ra_T = 10^7$, $Da = 10^{-5}$, $Le = 10$ and different values of N.

calculated and $\vec{n}$ is an unit normal to this surface.

5. Results

The obtained numerical algorithm has been used to investigate the three-dimensional flow structures and overall heat and mass transfer for different values of governing parameters: thermal Rayleigh number Ra_T, porous Rayleigh number Ra_P, Lewis number Le, Darcy number Da, buoyancy coefficient N, Prandtl number Pr, porosity ϕ and heat capacity ratio σ.

Firstly, the results for different grid sizes ($2D$ and $3D$) for an example when Ra_P=100, Le=0, N=0, Pr=0.71, $\phi = 0.8$, $\sigma = 1$ and various Da are shown in Table 1. Two nonuniform meshes for $2D$ case and four nonuniform meshes for $3D$ case have been tested. When comparing $2D$ and $3D$ results it can be seen, that for the case of low values of Darcy number $2D$ simulations underestimate the heat transfer up to 4.5%. The effect of three-dimensionality in dependence on different parameters is discussed below. However, the $3D$ results reveal, that the mesh $20 \times 8 \times 20$ with 28577 nodes provides acceptable accuracy and was chosen for the further computations.

The validation of numerical code has been primarily performed for purely thermal natural convection in porous cubic enclosure and compared to reference solutions available in the literature. In Table 2, the Nusselt number values for the case of 3D enclosure for Ra_P=1000, Pr=0.71, $\phi = 0.8$, $\sigma = 1$ and various Da are compared to solutions obtained by Sharma and Sharma [31]. The present results agree well with the data from the available literature, all Nusselt number values at different Darcy numbers are within 6% of the results in the reference study. The difference can be explained by the fact that in the study by Sharma and Sharma [31] the Darcy-Brinkman-Forchheimer model was used, where additional Forchheimer term includes inertial effects which occur at higher velocities. An inertial resistance term was not considered in the present study which results in higher values of Nu number when the values of Da number are low.

Furthermore, Tables 3–5 present the comparison results for the case of double-diffusive natural convection, where the buoyancy coefficient has negative values, $N < 0$, which means the thermal and solutal buoyancy forces are opposing each other. The results for different values of Ra_P, Da and Le are given, while the porous media properties are $\phi = 1$ and $\sigma = 1$, and Prandtl number is Pr=10. The agreement with reference solutions from [19] and [17] for all different governing parameters is very good.

The results of average Nusselt and Sherwood numbers at fix values of porosity, $\phi = 1$, heat capacity ratio $\sigma = 1$, Prandtl number Pr=10, thermal Rayleigh numbers $Ra_T = 10^5$, $Ra_T = 10^6$ and $Ra_T = 10^7$ at Lewis number Le=10, buoyancy coefficient N=1 and various Da are presented in Table 6. Values of Nu and Sh depend on the Ra_T, which directly influences the scale of the buoyancy term in Eq. (5) and Da, which influences the Darcy term in Eq. (5).

Further results are presented in Figs. 2 and 3, where the dependence of Nu and Sh on N is shown for fix values of $Ra_p = Ra_T \cdot Da = 100$, Le=10, various Da and N. Due to the boundary conditions considered in the present study, where the left-hand side vertical wall is maintained at higher temperature and concentration values as the right-hand side vertical wall, the resulting flow direction induced by thermal buoyancy forces is clockwise, while the direction of the solutal buoy-

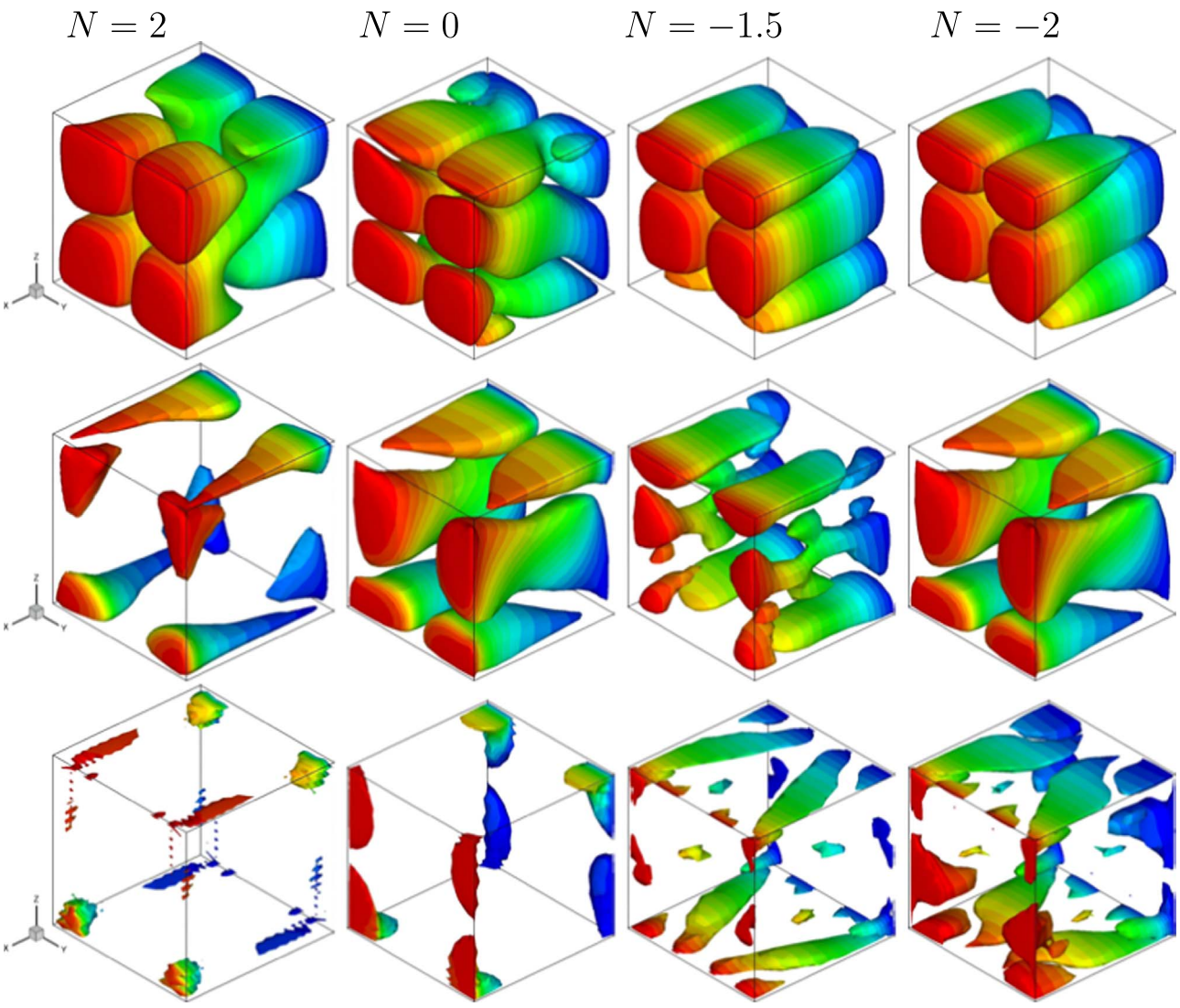

Fig. 11. Isosurfaces of $|v_y| = 0.1 v_{max}$ for $Ra_T = 10^3$ and $Da = 10^{-1}$ (upper row), $Ra_T = 10^5$ and $Da = 10^{-3}$ (middle row), $Ra_T = 10^7$ and $Da = 10^{-5}$ (bottom row), $Le = 10$ and different values of N with displayed contours of temperature ($-0.5 \leq T \leq 0.5$).

ancy forces depends on the sign of the buoyancy coefficient. When N=0, the only acting buoyancy forces are the thermal forces, the induced convection mechanism causes higher heat and mass transfer. With any increase of N in positive direction, the magnitude of convective motion becomes higher, which results in increased values of Nu and Sh numbers, at any value of Ra_T and Da. In case when $N < 0$, the direction of solutal buoyancy is opposing the thermal buoyancy, which at some critical point results in suppression of the convective motion. At $N = -1$, Nu and Sh values are lower than at any other value of N, which can be observed at any Da and Ra_T. At this point the thermal and solutal buoyancy effects neglect each other, which results in lower values of Nu and Sh. With further decrease of buoyancy coefficient, $-0.5 > N > -2$, the solutal buoyancy force becomes significant over the thermal one, which again increases the overall heat and mass transfer and results in higher values of Nu and Sh.

Under chosen geometry and boundary conditions, the buoyancy forces in the cavity induce the main vortex in the $x - z$ plane, so the plane $y = 0.5L$ is chosen to study temperature, concentration and velocity profiles. Figs. 4 and 5 show the temperature and concentration profiles at $y = 0.5L$ and $z = 0.5L$ for $Ra_T = 10^6$, Le=10, depending on Da and N. As expected, the highest temperature and concentration gradients can be observed near to the hot and the cold walls. Fig. 4 (a) and 5 (a) show that the temperature and concentration profiles at $N = -1.5$ and $N = -2$ are almost linear, which indicates that the main heat and solute transfer mechanism in this case is conduction. In Fig. 4 (b) and 5 (b) can be observed that at higher values of Da ($Da = 10^{-3}$) at fix Ra_T the temperature and concentration gradients are higher as in case of lower value of Da. In addition, vertical velocity profiles $v_z(x, 0.5L, 0.5L)$ and horizontal velocity profiles across the center of the cube are shown in Figs. 6 and 7. It is obvious that the fluid is moving faster along the vertical walls with applied values of temperature and concentration, where the velocity gradient is higher. The maximum values of the vertical velocity are closer to the wall in cases of high values of N (Fig. Fig. 6 (a)) and Da (Fig. Fig. 6 (b)), where the nonslip boundary condition prescribed on the vertical wall is almost violated.

Figs. 8, 9 and 10 show the streamlines, temperature fields and concentration fields for different values of N at Le=10 and $Ra_T = 10^3$, $Da = 10^{-1}$ (Fig. Fig. 8), $Ra_T = 10^5$, $Da = 10^{-3}$ (Fig. Fig. 9) and $Ra_T = 10^7$, $Da = 10^{-5}$ (Fig. Fig. 10). In case of low values od Ra_T and Da, the buoyancy forces are very weak; the isotherms are almost parallel to the vertical walls which indicates the dominating heat transfer mechanism is conduction. The convection becomes stronger with increasing the Ra_T and decreasing the Da (Figs. 9 and 10). In cases when $N < 0$, the change of direction of convective motion due to opposite acting of buoyancy forces can be observed in all fields. The

streamlines are closely spaces near the hot and cold walls, where the fluid is moving faster and the velocity gradient is higher. Larger absolute values of buoyancy ratio result in stronger convective motion which enhances heat and mass transfer in the cavity, in general.

In Fig. 11, the three dimensional structure of the flow field is shown for, Le=10 and different values of Ra_T, Da and N, where the iso-surfaces for absolute value of y velocity component are plotted. The value of $|v_y|$ is set to be 10% of the maximal fluid velocity for each case respectively, $|v_y| = 0.1v_{max}$. The y component of velocity is perpendicular to the plane of the main motion and is 0 in case when considering only $2D$ example. In general, the value of v_y is small in comparison to velocities in x and z directions, special at low Da values. In that case the 3D nature of the phenomena can be observed in the corners of the cubic cavity. Due to the fact that the flow field is driven by a large temperature and concentration difference between two opposite walls, which causes the main 2D vortex in the y plane, the flow structure in the enclosure remains mainly two-dimensional. However, with increase of Darcy number, the movement perpendicular to the plane of the main vortex becomes more apparent at any value of N.

6. Conclusions

In the present work a three-dimensional double-diffusive natural convection in porous enclosure is investigated numerically, using the algorithm which is based on the boundary element method. The mathematical model is based on the classical Navier-Stokes equations adopted for the porous media flow where the Brinkman-extended Darcy momentum equation is coupled with the energy and species equations. In order to use the boundary element method algorithm, the velocity-vorticity formulation of the governing equations was obtained, which separates the numerical scheme into the kinematic and kinetic computational parts. The boundary vorticity values were obtained from the single domain BEM solution of the kinematics equation, while the domain vorticity, temperature and concentration values, as well as domain velocity values were obtained by using the subdomain BEM.

The numerical code is validated by comparison of the results with some previously published numerical data available in the literature for different values of governing parameters. Further study is focused on the influence of a limited number of dimensionless parameters, namely the Rayleigh number, Darcy number and buoyancy coefficient. The results state specific behavior of double-diffusive flow in porous media; the heat and mass transfer strongly depend on Rayleigh Darcy numbers. Moreover, the increase of the absolute value of buoyancy coefficient enhances the overall heat and mass transfer, in general. In the range of the negative values of buoyancy coefficient, the thermal and solutal buoyancy effects start to oppose each other, which causes that the flow starts to flow in reversal direction. Three-dimensional nature of the flow relative on the velocity maximum can be observed at all different parameters and becomes more apparent at higher values of Darcy numbers.

References

[1] Murray BT, Chen CF. Double-diffusive convection in a porous medium. J Fluid Mech 1989;201:147–66.
[2] Trevisan OV, Bejan A. Combined heat and mass transfer by natural convection in a porous medium. Adv Heat Transf 1990;20:315–48.
[3] Rosenberg ND, Spera FJ. Thermohaline convection in a porous medium heated from below. Int J Heat Mass Transf 1992;35:1261–73.
[4] Amahmid A, Hasnaoui M, Mamou M, Vasseur P. Double-diffusive parallel flow induced in a horizontal brinkman porous layer subjected to constant heat and mass fluxes: analytical and numerical studies. Heat Mass Transf 1999;35:409–21.
[5] Mahidjiba A, Mamou M, Vasseur P. Onset of double-diffusive convection in a rectangular porous cavity subject to mixed boundary conditions. Int J Heat Mass Transf 2000;43:1505–22.
[6] Trevisan OV, Bejan A. Natural convection with combined heat and mass transfer buoyancy effects in a porous medium. Int J Heat Mass Transf 1985;28:1597–611.
[7] Trevisan OV, Bejan A. Mass and heat transfer by natural convection in a vertical slot filled with porous medium. Int J Heat Mass Transf 1986;29:403–15.
[8] Alavyoon F. On natural convection in vertical porous enclosures due to prescribed fluxes of heat and mass at the vertical boundaries. Int J Heat Mass Transf 1993;36:2479–98.
[9] Mamou M, Vasseur P, Bilgen E. Multiple solutions for double diffusive convection in a vertical porous enclosure. Int J Heat Mass Transf 1995;38:1787–98.
[10] Goyeau B, Songbe J-P, Gobin D. Numerical study of double-diffusive natural convection in a porous cavity using the Darcy-Brinkman formulation. Int J Heat Mass Transf 1996;39:1363–78.
[11] Nithiarasu P, Seetharamu KN, Sundararajan T. Double-diffusive natural convection in an enclosure filled with fluid-saturated porous medium: a generalized non-Darcy approach. Numer Heat Transf 1996;30:413–26.
[12] Karimi-Fard M, Charrier-Mojtabi MC, Vafai K. Non-Darcian effects on double-diffusive convection within a porous medium. Numer Heat Transf 1997;31:837–52.
[13] Bennacer R, Tobbal A, Beji H, Vasseur P. Double diffusive convection in a vertical enclosure filled with anisotropic porous media. Int J Therm Sci 2001;40:30–41.
[14] Kramer J, Jecl R, Škerget L. Boundary domain integral method for the study of double diffusive natural convection in porous media. Eng Anal Bound Elem 2007;31:897–905.
[15] Šarler B, Gobin D, Goyeau B, Perko J, Power H. Natural convection in porous media - dual reciprocity boundary element method solution of the Darcy model. Int J Numer Methods Eng 2000;33:279–312.
[16] Šarler B, Perko J, Gobin D, Goyeau B, Power H. Dual reciprocity boundary element method solution of natural convection in Darcy - Brinkman porous media. Eng Anal Bound Elem 2004;28:23–41.
[17] Sezai I, Mohamad AA. Three-dimensional double-diffusive convection in a porous cubic enclosure due to opposing gradients of temperature and concentration. J Fluid Mech 1999;400:333–53.
[18] Kramer J, Ravnik J, Jecl R, Škerget L. Three-dimensional double-diffusive natural convection with opposing buoyancy effects in porous enclosure by boundary element method. Int J Comput Methods Exp Meas 2013;1:103–15.
[19] Mohamad AA, Bennacer R, Azaiez J. Double diffusion natural convection in a rectangular enclosure filled with binary fluid saturated porous media: the effect of lateral aspect ratio. Phys Fluids 2004;16:184–99.
[20] Bear J. Dynamics of fluids in porous media. Mew York: Dover Publications, Inc.; 1972.
[21] Lauriat G, Prasad V. Natural convection in a vertical porous cavity: a numerical study for Brinkman-extended Darcy formulation. J Heat Transf 1987;109:688–96.
[22] Nield DA, Bejan A. Convection in porous media, third edition. Springer; 2006.
[23] Ravnik J, Škerget L, Hriberšek M. 2D velocity vorticity based LES for the solution of natural convection in a differentially heated enclosure by wavelet transform based BEM and FEM. Eng Anal Bound Elem 2006;30:671–86.
[24] Ravnik J, Škerget L, Žunič Z. Comparison between wavelet and fast multipole data sparse approximations for Poisson and kinematics boundary – domain integral equations. Comput Methods Appl Mech Eng 2009;198:1473–85.
[25] Ravnik J, Škerget L, Žunič Z. Velocity-vorticity formulation for 3D natural convection in an inclined enclosure by BEM. Int J Heat Mass Transf 2008;51:4517–27.
[26] Škerget L, Jecl R. Compressible fluid dynamics in porous media by the boundary element method. Emerg Technol Tech Porous Media 2003.
[27] Ravnik J, Škerget L, Žunič Z. Combined single domain and subdomain BEM for 3D laminar viscous flow. Eng Anal Bound Elem 2009;33:420–4.
[28] Ravnik J, Škerget L, Hriberšek M. Analysis of three-dimensional natural convection of nanofluids by BEM. Eng Anal Bound Elem 2010;34:1018–30.
[29] Wrobel LC. The Boundary Element Method. John Willey & Sons, LTD; 2002.
[30] Kramer J, Ravnik J, Jecl R, Škerget L. Simulation of 3D flow in porous media by boundary element method. Eng Anal Bound Elem 2011;35:1256–64.
[31] Sharma RV, Sharma RP. Non-Darcy effects on three-dimensional natural convection in a porous box. Annals of the Assembly for International Heat Transfer Conference 13, 0:NCV–10, 2006.